

## Design and performance enhancement of a modified corrugated Vivaldi micro-strip patch antenna for remote sensing applications

Betül Yılmaz\*<sup>1</sup> , Caner Özdemir<sup>1</sup> 

<sup>1</sup> Mersin University, Faculty of Engineering, Department of Electrical and Electronics Engineering, Mersin, Türkiye; betuly@mersin.edu.tr; cozdemir@mersin.edu.tr



### Article History:

Received: 16 March 2025  
Revised: 6 April 2025  
Accepted: 16 April 2025  
Published: 30 June 2025



**Copyright:** © 2025 by the authors.

This article is an open access article distributed under terms and conditions of the Creative Commons Attribution (CC BY-SA) license. <https://creativecommons.org/licenses/by-sa/4.0/>

**Abstract:** In this study, a practical modified corrugated Vivaldi micro-strip patch antenna (MC-VMSPA) is designed for the use of remote sensing applications such as through-wall radar applications. First, the basic design of Vivaldi micro-strip patch antenna (VMSPA) is optimized for the targeted band of frequencies of the through-wall radar applications. Then, a modified design that consists of a series of parasitic radiating patches on the substrate antenna is proposed to enhance the operational bandwidth of the radar and to attain the required directiveness with a practical gain value. The outcome after the design and the optimization of the proposed antenna is presented in comparison with the classical VMSPA. Analyzing the optimized design in terms of antenna parameters demonstrates the effectiveness and the availability of the designed MC-VMSPA for the use of remote sensing radar applications.

**Keywords:** Remote sensing; Vivaldi antenna; modified corrugated Vivaldi

**Citation:** Yılmaz, B., & Özdemir, C. (2025). Design and performance enhancement of a modified corrugated Vivaldi micro-strip patch antenna for remote sensing applications. *Turk. J. Remote Sens.*, 7(1), 43-52. <https://doi.org/10.51489/tuzal.1658945>

## 1. Introduction

Through-wall imaging radar (TWIR) technology necessitates various aspects of the radar antenna including ultrawide-band operation for sharp resolution in range, and high directivity for better penetration on different wall materials (Kuriakose et al., 2020; Yang et al., 2021; Yılmaz, 2023; Zhu et al., 2011). For these reasons, several antennas have been proposed by different researchers in various usages (Karanth et al., 2017; Pieraccini et al., 2018; Hariyadi et al., 2016; Pinchera et al., 2013). Among directive antennas, Vivaldi type micro-strip patch antennas (VMSPA) seem to be suitable for TWIR applications since they can provide high gain, relatively narrower main beam, directional antenna pattern and ultrawideband (UWB) operation (Zhang et al., 2020; Tahar et al., 2018). Additional to these attractive features, they are also light-weight, simple and usually very economical to manufacture. Corrugated version of VMSPA presents improvements on the antenna parameters including directivity and the operational bandwidth. Hence, different designs of this type of antenna have been studied recently by various researchers (Ahmed & Hassain, 2020; Pandey et al., 2015; Paul et al., 2023).

Paul et al. (2023) has designed UWB slotted Vivaldi antenna for microwave imaging (MI) applications. Although the antenna could provide UWB operation with about 10 GHz bandwidth, its maximum gain is limited to 7.35 dB. For TWIR applications, where electromagnetic (EM) wave experiences significant attenuation as they propagate through different materials, a higher gain would be more advantageous to ensure better signal penetration. Pandey et al. (2015) enhanced a compact UWB Vivaldi antenna by incorporating corrugations and three metal strips that act like Yagi-Uda directors to improve directivity. While this antenna has a wide bandwidth from 2.9 GHz to 11 GHz, its gain varies from 4.5 dBi

to 8 dBi. Although this design increases radiation performance, achieving even higher gain could be beneficial for applications requiring greater signal penetration (Pandey et al., 2015). For radar and MI applications operating within 2.7 GHz to above 12 GHz, a gain-enhanced UWB tapered slot Vivaldi antenna (TSVA) was designed by Ahmed & Hassain (2020). In their study, a polygonal dielectric lens and three metallic rectangular directors of unequal length were combined to improve the antenna performance. These modifications helped to increase the bandwidth while keeping the gain below 10 dB.

In this work, we introduce a novel design for the different design of the corrugated VMSPA (C-VMSPA) by introducing a series of parasitic radiating patches on the classical design of C-VMSPA. The organization of the paper is as follows: In Sect. II, we begin with a standard design based on the basic C-VMSPA type to provide the baseline for our proposed antenna. The antenna parameter simulation has also been done using CST Microwave Studio Software (CST, 2016). In the next section, we introduce the proposed design for the modified C-VMSPA (MC-VMSPA) model together with the antenna simulations and analyses. The comparison of the new antenna simulations with the classical one is presented to reflect the improvements gained by the modified design of C-VMSPA. In the last section, the work is summarized and the use of this antenna for future remote sensing radar applications is discussed.

## 2. The Design and Simulation of C-VMSPA for TWIR Bands

### 2.1. C-VMSPA antenna geometry

The proposed C-VMSPA is designed utilizes an FR4 substrate with a standard thickness of 1.5 mm, relative permittivity of 4.35 and tangent loss of 0.025 and features a microstrip patch structure that follows an exponentially tapered transmission line in both vertical and horizontal directions which plays a crucial role in achieving UWB operation and directional radiation characteristics. The exponential curve defining the flare profile is given by (Paul & Islam, 2021).

$$Y(x) = K_1 e^{rx} + K_2, \quad (1)$$

where  $Y(x)$  represents the slot width at a given position  $x$ ,  $K_1$  and  $K_2$  are given by;

$$K_1 = \frac{y_2 - y_1}{e^{rx_1} - e^{rx_2}} \quad (2)$$

$$K_2 = \frac{e^{rx_2} y_1 - e^{rx_1} y_2}{e^{rx_2} - e^{rx_1}} \quad (3)$$

In Equation (1),  $K_1$  and  $K_2$  are constants that define the geometric constraints of the structure, while  $r = 0.3$  represents the growth rate of the exponential curve. The parameters  $(x_1, y_1)$  and  $(x_2, y_2)$  correspond to the initial and termination points of the curve, respectively, governing the spatial expansion of the tapered profile. These parameters collectively influence the impedance matching and radiation characteristics of the antenna, ensuring efficient wave propagation across a broad frequency range. The addition of rectangular corrugations along the slot edges improves impedance matching, reduces side lobe levels, and enhances directivity by suppressing surface wave propagation. The corrugated edges contribute to better phase coherence, ensuring stable radiation patterns across a broad frequency range. Figure 1 shows that optimized dimension of the C-VMSPA geometry having rectangular corrugations along the slot edges.

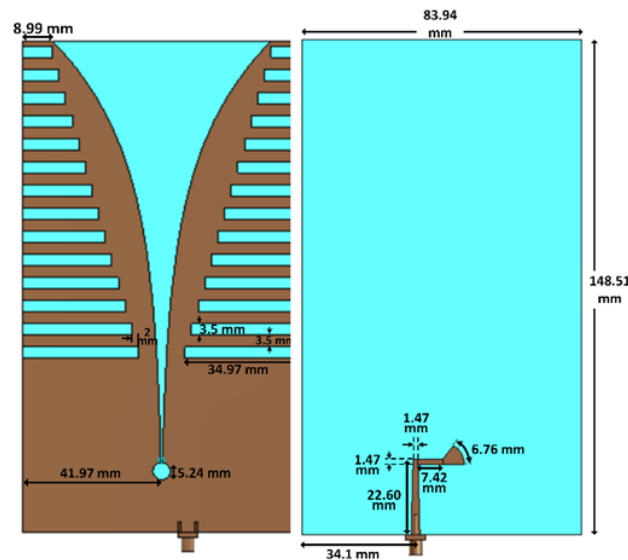


**Figure 1.** Optimized dimension of the C-VMSPA geometry having rectangular corrugations along the slot edges

The corrugation slots are individually optimized to achieve the desired impedance matching by carefully adjusting their dimensions and placement along the antenna structure. To determine the optimal locations of these corrugations, a comparative current distribution analysis is conducted for both the non-corrugated; VMSPA and corrugated configurations C-VMSPA, as illustrated in Figure 2.

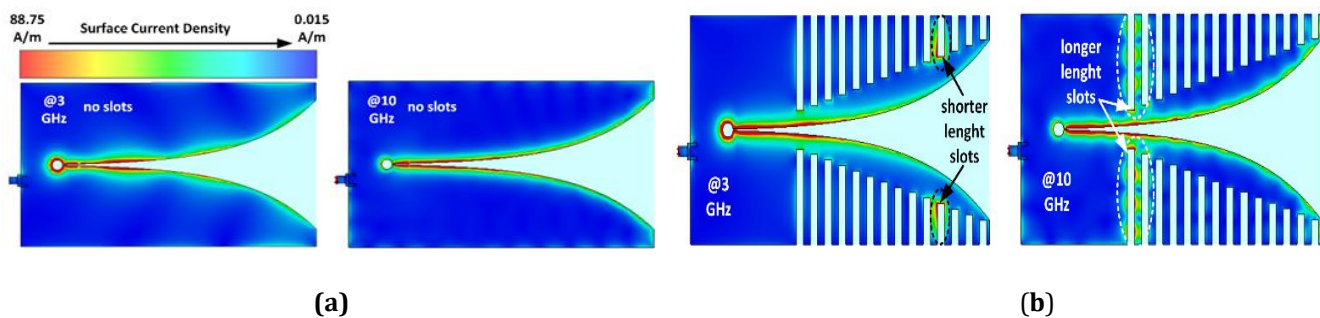


**Figure 2.** Surface current distributions at 3 GHz and 10 GHz for (a) VMSPA (b) C-VMSPA

From surface current distribution plots in Figure 2(a), the following deductions can be observed for the conventional VMSPA: Surface current is concentrated along the inner edge of the exponentially tapered line and around the cavity at lower and higher frequencies at 3 GHz and 10 GHz. Incorporating corrugations into the structure increases the electrical length, generating additional resonances. Each corrugation resonates at a different frequency, effectively redistributing the current along its perimeter. When surface current distribution figures are assessed via Figure 2(b) for the C-VMSPA, one can easily note the following: The current is primarily concentrated around the shorter-length slot at the lower frequency of 3 GHz, whereas it predominantly builds up around the longer-length slot at the higher frequency of 10 GHz. Hence, corrugations play a crucial role in enhancing the bandwidth by improving the impedance matching and introducing additional resonances. The antenna is fed through a standard 50 Ω SMA connector, transmitting the signal along the micro-strip line. As observed in Figure 3, the reflection coefficient ( $S_{11}$ ) illustrates the impedance matching performance and operational bandwidth for both the VMSPA and the C-VMSPA. The conventional VMSPA exhibits an impedance bandwidth spanning from 2.64 to 10.64 GHz; however, it stays above -10 dB level at certain frequencies within the 3 – 4.5 GHz and

6.5 – 8 GHz ranges, indicating suboptimal impedance matching in these regions. On the other hand, the CVMSPA improves impedance matching, especially within the lower frequency range, resulting in a wider operating bandwidth from 2.35 to 10.6 GHz. However, in the 7– 8 GHz frequency range, the C-VMSPA still exhibits a  $S_{11}$  performance above -10 dB (rising to approximately -8 dB level), suggesting that further design refinements may be needed to improve impedance matching in this region.

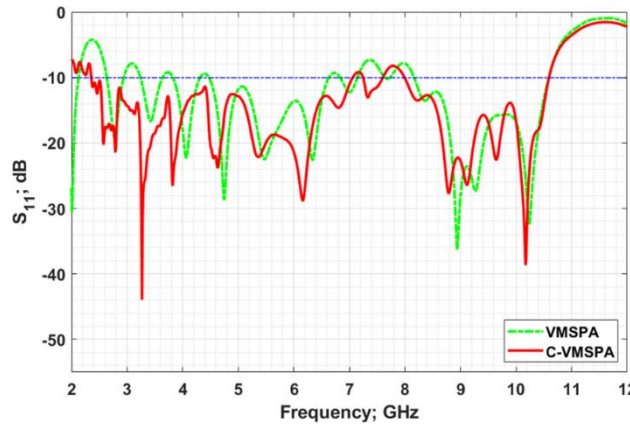


**Figure 3.** Comparison of reflection coefficient ( $S_{11}$ ) performances of the VMSPA and C-VMSPA

The far-field radiation pattern is a critical parameter in evaluating the overall performance of an antenna, as it directly influences the antenna’s directivity, beam width, and side lobe suppression ability, all of which are essential for efficient transmission and reception of the signal. Figures 4(a) and 4(b) illustrate the radiation patterns of the C-VMSPA at the center frequency of  $f_c = 6.475$  GHz for the E-plane and H-plane, respectively. In the E-plane, the main lobe magnitude is measured as 9.37 dBi, with a half-power beam width (HPBW) of 68.0°, and a side lobe level (SLL) of -7.6 dB. Similarly, in the H-plane, the main lobe amplitude reaches to 9.38 dBi, with an HPBW of 56.0° and an SLL of -8.7 dB. Although these characteristics indicate a well-defined directional radiation pattern with moderate beam width and controlled side lobes, further performance enhancement is necessary for TWIR applications, where higher gain is essential to ensure deeper penetration and stronger signal reflection from targets.

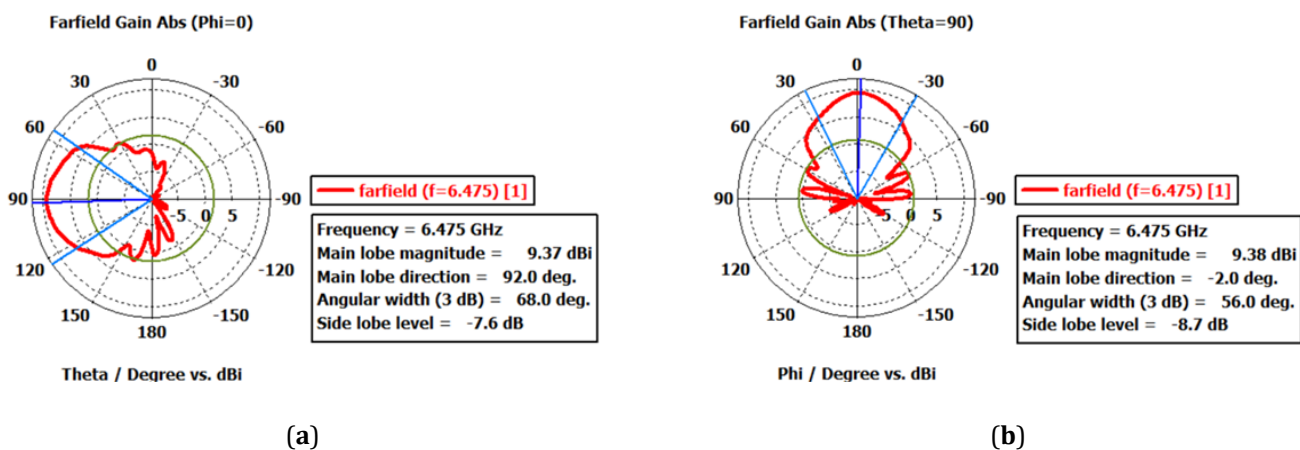


**Figure 4.** Radiation pattern performance at 6.475 GHz for the (a) E-plane and (b) H-plane of the C-VMSPA.

### 3. The Design and Simulation of MC-VMSPA for TWIR Bands

To enhance the antenna performance of C-VMSPA, novel structural modifications have been implemented to refine the antenna's frequency response. Specifically, circular slots have been introduced in the radiating patch to optimize current distribution and reduce the

impedance mismatches, thereby improving the return loss in the affected frequency region. Additionally, the integration of C-shaped metallic structures in a periodic arrangement plays a crucial role in enhancing the performance of the C-VMPA by introducing additional resonance modes and improving impedance matching across a wide frequency range. The optimization of their dimensions and placement is essential to achieving the desired electromagnetic properties, as it directly influences the antenna's gain, bandwidth, and radiation characteristics. By strategically positioning these resonators along the substrate, surface wave suppression is enhanced, leading to better directivity. Furthermore, the periodic configuration aids in effectively guiding and concentrating the radiated energy, thereby increasing the antenna's efficiency in end-fire radiation. This structural enhancement not only improves the overall return loss by mitigating impedance mismatches but also contributes to higher gain and stable radiation patterns, making the antenna highly suitable for applications such as TWIR, where strong signal penetration and high-resolution imaging are essential. Figure 5 illustrates the final modified corrugated Vivaldi micro-strip antenna (MC-VMSPA) geometry, incorporating C-shaped metallic resonators and circular slots to enhance impedance matching, bandwidth, and radiation performance. Table 1 presents the optimized design dimensions related to C-shaped metallic resonators and twin circular slots, which have been determined through an extensive optimization process to achieve the best impedance matching, bandwidth, and radiation performance.

**Table 1.** The optimized design dimensions of the C-shaped metallic resonators and circular slots

Symbol	Explanation	Value
D	open aperture of "C" element	1.1 mm
W	width of rectangular slot within "C" element	1.5 mm
L	length of rectangular slot within "C" element	1.8 mm
R <sub>c</sub>	radius of "C" element	3.6 mm
R	radius of twin circular slots	24 mm
R <sub>1</sub>	distance of first "C" element from cavity center	79.35 mm
N	Number of "C" elements	14
d <sub>h</sub>	spacing between the horizontal axis of "C" elements	8 mm
d <sub>v</sub>	spacing between the vertical axis of "C" elements	6.8 mm

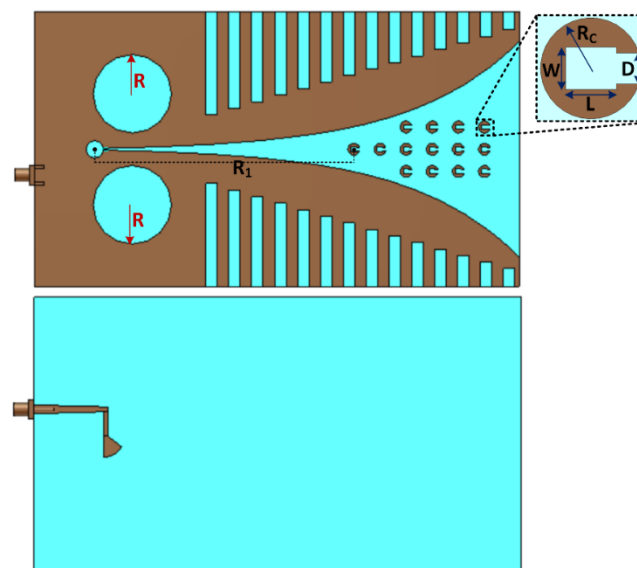


**Figure 5.** The final optimized MC-VMSPA geometry

Figure 6 shows the surface current distribution of the MC-VMSPA at 3 GHz, 8 and 10 GHz. In the MC-VMSPA structure, it is observed that the maximum current density increases at all frequencies compared to the CVMSPA. At 3 GHz, the current is still concentrated around relatively short corrugations, similar to CVMSPA, but with a higher intensity. However, there

is a significant shift at 8 GHz, with the current concentrating around the longer corrugations rather than at 10 GHz, indicating a possible shift in the resonant frequency. In addition, the C-shaped resonators introduced in the MCVMSPA show a noticeable magnitude of current distribution, particularly at 10 GHz, where a significant concentration around these resonators is observed. These results suggest that the incorporation of C-shaped resonators and modified corrugations alters the current distribution, potentially improving impedance matching and introducing new resonances, thereby affecting the operational bandwidth and frequency response of the antenna.

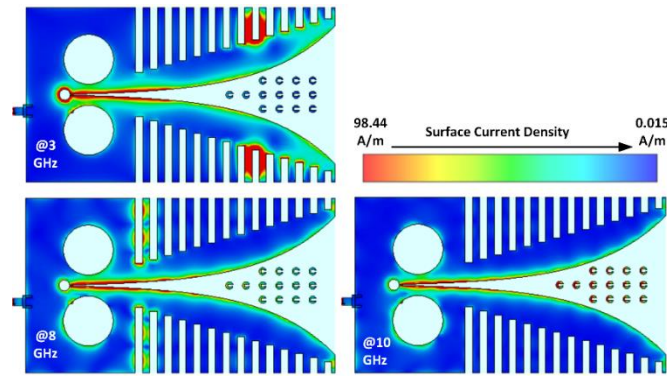


**Figure 6.** Surface current distributions at 3 GHz, 8 GHz and 10 GHz for MC-VMSPA

Figure 7 illustrates the  $S_{11}$  performance of the MC-VMSPA, demonstrating a significant improvement over the initial design. In the primary C-VMSPA, a noticeable impedance mismatch was observed between 7 and 8 GHz, where the return loss was around  $-8$  dB. However, the modified design successfully maintains return loss below  $-10$  dB over the entire operating bandwidth from 2.35 to 10.70 GHz, eliminating the previous impedance mismatch and providing improved impedance continuity. The fractional bandwidth calculated as and exceeds the UWB definition of 20%; thus, the modified antenna warrants outstanding UWB operation. This improvement is attributed to the incorporation of C-shaped metallic resonators and circular slots, which effectively introduce additional resonance modes, refine the current distribution, and enhance impedance matching across UWB spectrum.

$$FBW = \frac{BW}{f_c} = \frac{8.35 \text{ GHz}}{(10.7 \text{ GHz} + 2.35 \text{ GHz})/2} \times 100 \cong 112.8\% \tag{4}$$

and exceeds the UWB definition of 20%; thus, the modified antenna warrants outstanding UWB operation. This improvement is attributed to the incorporation of C-shaped metallic resonators and circular slots, which effectively introduce additional resonance modes, refine the current distribution, and enhance impedance matching across UWB spectrum.

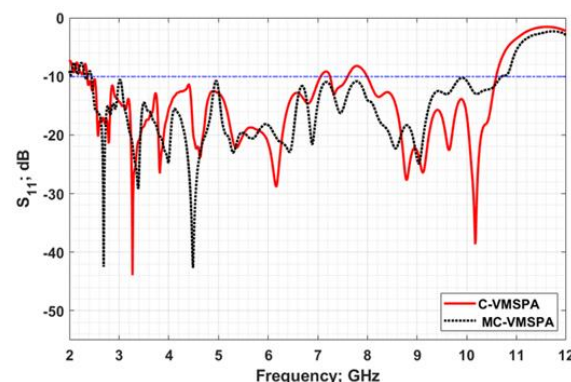


**Figure 7.** Comparison of reflection coefficient ( $S_{11}$ ) performances of the C-VMSPA and MC-VMSPA

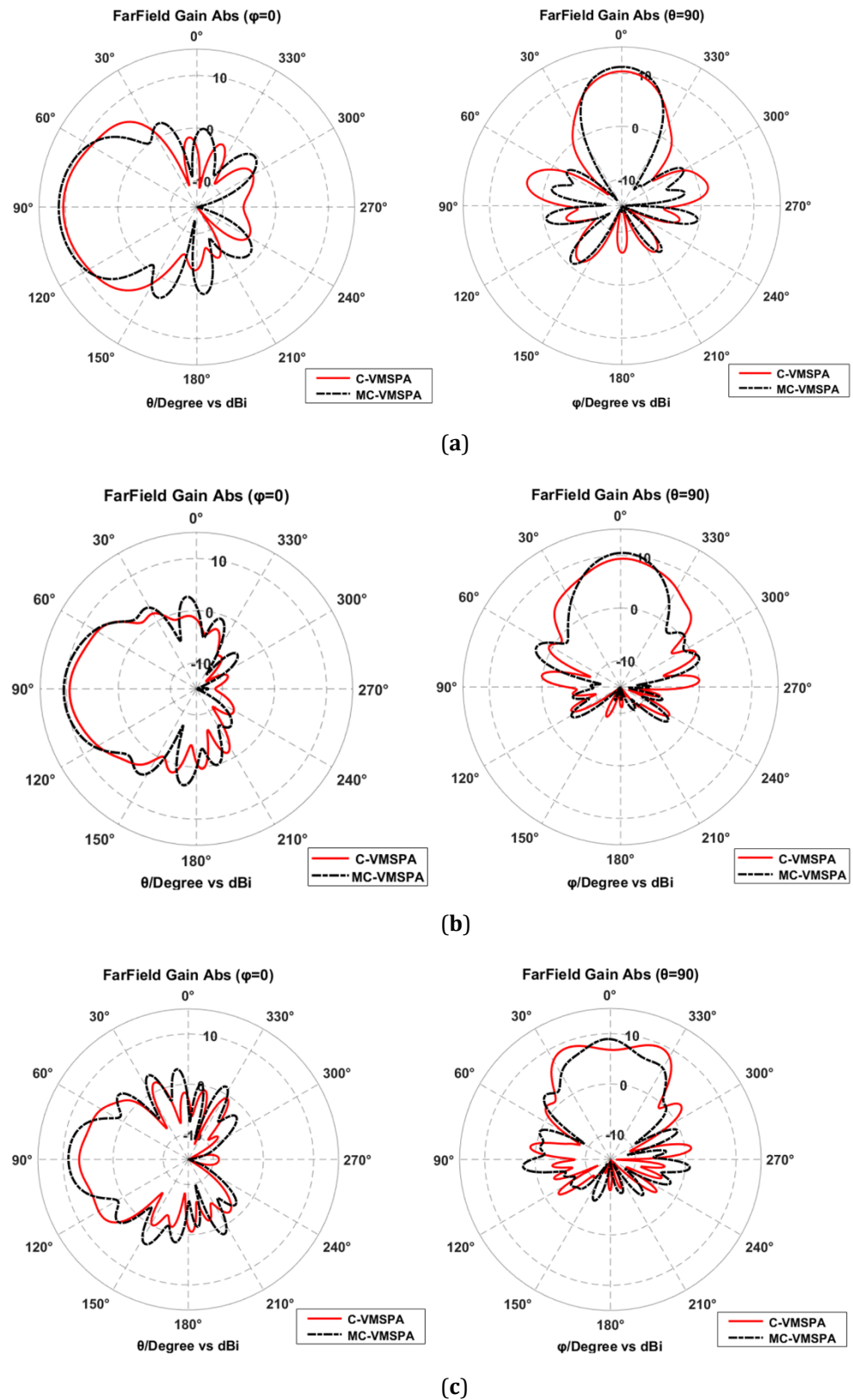


**Figure 8.** The E-plane [ $\varphi=0$ ] and H-plane [ $\varphi=90$ ] radiation patterns of the C-VMSPA and MC-VMSPA at (a) 5 GHz, (b) 6.475 GHz (center frequency) and (c) 8 GHz

In Figure 8, The E-plane [ $\varphi=0$ ] and H-plane [ $\varphi=90$ ] radiation patterns of the C-VMSPA and MC-VMSPA are presented at which significant improvements have been accomplished after modifications compared to initial design of C-VMSPA. Radiation pattern results at 5 GHz, 6.475 GHz and 8 GHz are presented in Figure 8(a), (b), and (c), respectively. In the E-plane ( $\varphi = 0^\circ$ ) at the center frequency of 6.475 GHz, the gain has increased to 10.5 dBi, with a

HPBW of 59.9° and a SLL of -5.8 dB is shown in left side of the Figure 8(b). Compared to the former design of C-VMSPA, where the HPBW was 68.0° and the SLL was -7.6 dB, the modified structure provides a narrower main beam, resulting in improved directivity at the expense of slightly higher side lobe levels.

The H-plane ( $\theta = 90^\circ$ ) radiation pattern is illustrated on the right side of the Figure 8(b), the gain remains at 10.5 dBi, while the HPBW is reduced to 37.8°, significantly narrower than that of the previous C-VMSPA design, which was 56.0°. Despite the -7.8 dB SLL, the antenna exhibits a narrower HPBW and a higher gain, indicating improved directivity. The reduction in beam-width, especially in the H-plane, suggests that the modified antenna exhibits better focused radiation pattern, which is particularly beneficial for TWIR applications, where higher gain and improved directivity are the critical parameters for enhancing electromagnetic wave penetration and radar imaging resolution. These results confirm that the introduction of C-shaped metallic resonators and circular slots has led to a more directional and efficient radiation performance, making the antenna better suited for high-precision sensing and imaging applications. Table 2 depicts the comparisons of gain, HPBW and SLL for the E-plane and H-plane radiation patterns at the lower, center and upper frequencies of the operational band.

**Table 2.** Radiation pattern parameter comparison for the C-VMSPA and MC-VMSPA

Parameter	E-Plane [ $\varphi = 0^\circ$ ]		H-Plane [ $\theta = 90^\circ$ ]		
	C-VMSPA	MC-VMSPA	C-VMSPA	MC-VMSPA	
Gain	@ 5 GHz	10.38 dBi	11.24 dBi	10.40 dBi	11.20 dBi
	@ 6.475 GHz	9.37 dBi	10.50 dBi	9.38 dBi	10.50 dBi
	@ 8 GHz	6.76 dBi	8.90 dBi	6.75 dBi	8.92 dBi
HPBW	@ 5 GHz	82.1°	66.0°	37.0°	33.9°
	@ 6.475 GHz	68.0°	59.9°	56.0°	37.8°
	@ 8 GHz	77.9°	41.0°	67.7°	54.5°
SLL (max)	@ 5 GHz	-12.0 dB	-7.5 dB	-6.9 dB	-11.7 dB
	@ 6.475 GHz	-7.6 dB	-5.8 dB	-8.7 dB	-7.8 dB
	@ 8 GHz	-5.1 dB	-5.0 dB	-6.7 dB	-5.8 dB

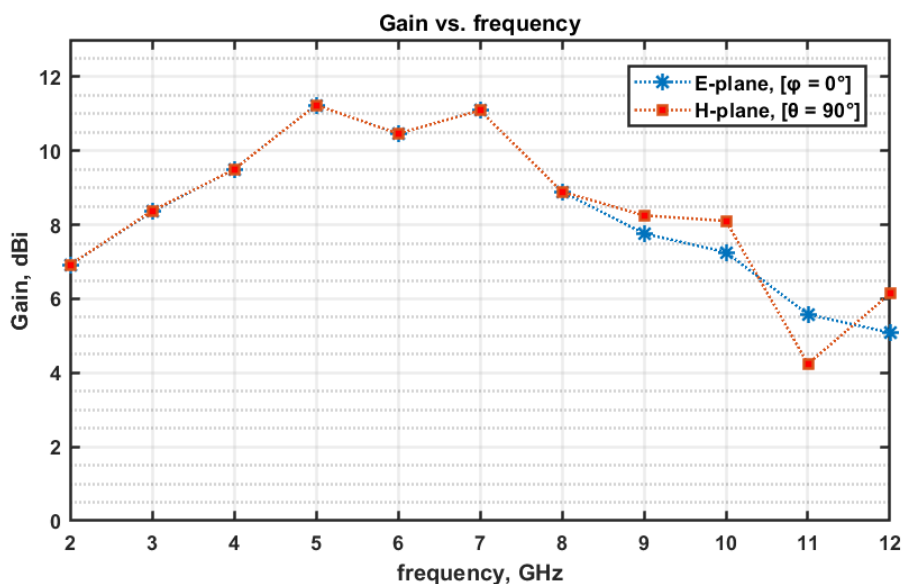


**Figure 9.** Gain plot of the MC-VMSPA over the 2–12 GHz frequency range: E-plane [ $\varphi = 0^\circ$ , blue dashed line with solid circle markers] and H-plane [ $\theta = 90^\circ$ , red dashed line with solid circle markers].

The MC-VMSPA is tailored for UWB-TWIR applications where wide frequency coverage is essential for high resolution performance. Therefore, the gain performance of the MC-VMSPA has been plotted over the 2-12 GHz range for both the E-plane ( $\varphi = 0^\circ$ ) and the H-plane ( $\theta = 90^\circ$ ) in Figure 9. This provides a clear illustration of the broadband radiation behavior of the antenna, confirming its suitability for UWB through-wall imaging radar applications.

#### 4. Discussion and Conclusions

The proposed antenna, with its high performance, offers significant potential not only for TWIR applications, but also for various remote sensing usages. With its high gain and directivity features, the antenna can provide accurate target detection in challenging environments, including behind opaque obstacles. Therefore, the proposed antenna holds great promise for a wide range of detection, classification and surveillance applications. Future research could explore the integration of machine learning and artificial intelligence algorithms, which could further enhance the antenna's detection accuracy and target classification capabilities.

This paper presents a comprehensive analysis of the MC-VMSPA design based on CST simulations. In this study, it was demonstrated that MC-VMSPA has shown significant performance improvements over the original C-VMSPA design, obtained using CST, particularly in terms of impedance matching, radiation characteristics, and directivity. Through the strategic integration of C-shaped metallic resonators and circular slots, the antenna achieves an expanded operational bandwidth, with acceptable impedance matching performance across the whole frequency band, ensuring efficient signal transmission. The far-field radiation patterns in both the E- and H-planes reflect improved directivity and a more focused radiation beam, which are critical for applications such as TWIR. These improvements lead to better control over side lobes and a more concentrated main lobe, enhancing the antenna's ability to penetrate through obstacles with minimal interference. In addition, the CST-based gain plot of the MC-VMSPA over the frequency range from 2 to 12 GHz highlights its broadband radiation performance and confirms its suitability for ultra-wideband applications. Overall, the optimized structure not only provides a broader operational bandwidth but also offers superior radiation performance, making it well-suited for high-resolution imaging and sensing applications, particularly in environments requiring precise and stable signal reception, such as in radar-based imaging systems.

---

##### Author Contributions:

B. Yilmaz: Writing—review & editing, Writing—original draft, Validation, Software, Resources, Methodology, Investigation, Formal analysis, Conceptualization.

C. Özdemir: Writing —review & editing, Writing—original draft, Software, Resources, Methodology, Supervision, Conceptualization.

**Research and publication ethics statement:** In the study, the authors declare that there is no violation of research and publication ethics and that the study does not require ethics committee approval.

**Conflicts of Interest:** The authors declare no conflicts of interest.

---

#### References

- Ahmed, S. K., & Hassain, Z. A. A. (2020). Gain enhancements of tapered slot Vivaldi antenna for radar imaging applications. *International Journal of Physics: Conference Series*, 1530, 1-11. <https://doi.org/10.1088/1742-6596/1530/1/012074>
- CST. (2016). CST Microwave Studio. Retrieved December 8, 2016, from <https://www.3ds.com/products-services/simulia/products/cst-studio-suite>
- Hariyadi, T., Huda, Y. T., & Mulyanti, B. (2016). A small ultra-wideband unidirectional microstrip antenna for through-wall radar application. *Journal of Telecommunication, Electronic and Computer Engineering (JTEC)*, 8(1), 25-28.

- Karanth, A., Onkar, N., Smitha, N. S. N., Sridhara & Singh, V. (2017, January 06-07). Through-wall imaging system using horn antennas [Paper presentation]. 4th International Conference on Advanced Computing and Communication Systems (ICACCS), Coimbatore, India, 1-6. <https://doi.org/10.1109/ICACCS.2017.8014591>
- Kuriakose, A., George, T. A. & Anand, S. (2020, December 14-16). Improved high gain Vivaldi antenna design for through-wall radar applications [Paper presentation]. International Symposium on Antennas & Propagation (APSYM), Cochin, India, <https://doi.org/10.1109/APSYM50265.2020.9350711>
- Pandey, G. K., Singh, H. S., Bharti, P. K., Pandey, A., & Meshram, M. K. (2015). High gain Vivaldi antenna for radar and microwave imaging applications. *International Journal of Signal Processing Systems*, 3(1), 35-39. <https://doi.org/10.12720/ijsp.3.1.35-39>
- Paul, L. C., & Islam, Md. M. (2021). A Super wideband directional compact Vivaldi antenna for lower 5G and satellite applications. *International Journal of Antennas and Propagation*, 2021(1). <https://doi.org/10.1155/2021/8933103>
- Paul, L. C., Majumder, A., Rani, T., Hossain, N., Rahim, A., Shin, J., & Yun, K. S. (2023). Design and analysis of a UWB slotted Vivaldi antenna for microwave imaging applications. *IEIE Transactions on Smart Processing & Computing*, 12(4), 350-357. <https://doi.org/10.5573/IEIESPC.2023.12.4.350>
- Pieraccini, M., Miccinesi, L., & Rojhani, N. (2018, September). Comparison between horn and bow-tie antennas for through-the-wall applications [Paper presentation]. IEEE Conference on Antenna Measurements & Applications (CAMA), Västerås, Sweden. <https://doi.org/10.1109/CAMA.2018.8530531>
- Pinchera, D., Migliore, M. D., & Schettino, F. (2013). An ultra wide permittivity antenna (UWPA) for reliable through-wall communications. *IEEE transactions on antennas and propagation*, 61(2), 957-960. <https://doi.org/10.1109/TAP.2012.2223439>
- Tahar, Z., Dérobert, X., & Benslama, M. (2018). An ultra-wideband modified vivaldi antenna applied to through the ground and wall imaging. *Progress In Electromagnetics Research C*, 86, 111-122. <https://doi.org/10.2528/PIERC18051502>
- Yang, D., Zhu, Z., Zhang, J., & Liang, B. (2021). The overview of human localization and vital sign signal measurement using handheld IR-UWB through-wall radar. *Sensors*, 21(2), 402. <https://doi.org/10.3390/s21020402>
- Yilmaz, B. (2023). Design of ultra-wide band dual-polarized quad ridged horn antenna for obstacle penetrating radar imaging applications. *International Journal of Engineering and Geosciences*, 8(1), 76-82. <https://doi.org/10.26833/ijeg.1053213>
- Zhang, J., Lan, H., Liu, M., & Yang, Y. (2019). A handheld nano through-wall radar locating with the gain-enhanced Vivaldi antenna. *IEEE Sensors Journal*, 20(8), 4420-4429. <https://doi.org/10.1109/JSEN.2019.2963234>
- Zhu, F., Gao, S., Ho, A. T. S., Brown, T. W. C., Li, J. Z., & Xu, J. D. (2011). Low-profile directional ultra wide band antenna for see-through-wall imaging applications. *Progress In Electromagnetics Research*, 121, 121-139. <https://doi.org/10.2528/PIER11080907>